Biomaterials Science

ROYAL SOCIETY OF CHEMISTRY

PAPER

View Article Online
View Journal | View Issue

Cite this: *Biomater. Sci.*, 2022, **10**, 3540

One-pot bifunctionalization of silica nanoparticles conjugated with bioorthogonal linkers: application in dual-modal imaging†

Jaewoon Lee,‡[a,b] Jeunghwan Kim,‡[a,b] Incheol Heo,[a,b] Su Jin Kim,[c] Sein Jang,[b,d] Ho-Young Lee,[c] Kwang-Suk Jang,[a,b,e] Chul-Su Yang,[b,d] Youngbok Lee,[a,b,e] Won Cheol Yoo[a,b,e] and Sun-Joon Min*[a,b,e]

Received 21st February 2022, Accepted 3rd May 2022

DOI: 10.1039/d2bm00258b

rsc.li/biomaterials-science

Covalent surface modification of silica nanoparticles (SNPs) offers great potential for the development of multimodal nanomaterials for biomedical applications. Herein, we report the synthesis of covalently conjugated bifunctional SNPs and their application to *in vivo* multimodal imaging. Bis(methallyl)silane **15** with cyclopropene and maleimide, designed as a stable bifunctional linker, was efficiently synthesized by traceless Staudiger ligation, and subsequently introduced onto the surface of monodispersed SNPs *via* Sc$(OTf)_3$-catalyzed siloxane formation. The bifunctional linker-grafted SNP **20** underwent both thiol-conjugated addition and tetrazine cycloaddition in *one pot*. Finally, positron emission tomography/computed tomography and fluorescence imaging study of dual functional SNP **[^{125}I]28** labeled with NIR dye and ^{125}I isotope showed a prolonged circulation in mice, which is conducive to the systemic delivery of therapeutics.

Introduction

Nanomaterials have been used in a wide range of biomedical applications, including drug delivery, diagnostics, and therapy.[1] In recent years, well-designed nanoparticles including gold nanoparticles, quantum dots, polymer nanoparticles, liposomes, and carbon nanotubes[2] have been developed, many of which showed selective, high efficacy delivery of a drug or an imaging agent into its target. Among the various nanocomposites, silica nanoparticles (SNPs) have been investigated extensively as nanomedicinal platforms owing to advantages such as controllable sizes and shapes, easy surface modification, biocompatibility, and biodegradability.[3] In general, functionalized SNPs are prepared by either physical absorption or covalent bonding. Various functional molecules are easily introduced into the inner space of SNPs by physical doping, but this method is not useful because its loading efficiency is low owing to the easy desorption of the doped material.[4] Alternatively, covalent conjugation of cargo molecules with SNPs enhances nanoparticle stability and prevents SNP cargo from being unexpectedly released.[5] Typically, cargo molecules are prefunctionalized with siloxanes, which are incorporated into the SNPs by conjugation with surface silanol groups. In this process, it is very common to use organoalkoxysilanes containing terminal nucleophilic groups, such as (3-aminopropyl)triethoxysilane (APS) or (3-mercaptopropyl)trimethoxysilane (MPS), as precursors (Fig. 1a). Although various diagnostic or therapeutic agents have been successfully integrated into the surface of SNPs *via* covalent bonding, applicable reactions for the synthesis of functionalized organosilanes are limited because of the easy hydrolysis of alkoxysilane. In addition, this process is unsuitable for the preparation of multimodal SNPs because different types of alkoxysilanes cannot be grafted onto the surface of SNPs in a single synthetic step.

Recently, allylsilanes have been used as precursors for the surface modification of silica by several research groups.[6,7] Compared to alkoxysilanes, allylsilanes are highly stable and can be purified by column chromatography on silica gel, and they are efficiently introduced into silica under refluxing conditions or in the presence of Lewis acid catalysts. In particular, various functional groups such as halides, aldehydes, cya-

[a]Department of Applied Chemistry, Hanyang University, Ansan, Gyeonggi-do, 15588, Republic of Korea. E-mail: sjmin@hanyang.ac.kr
[b]Center for Bionano Intelligence Education and Research, Hanyang University, Ansan, Gyeonggi-do, 15588, Republic of Korea
[c]Department of Nuclear Medicine, Seoul National University Bundang Hospital, Seongnam, Gyeonggi-do, 13620, Republic of Korea
[d]Department of Molecular and Life Science, Hanyang University, Ansan, Gyeonggi-do, 15588, Republic of Korea
[e]Department of Chemical & Molecular Engineering, Hanyang University, Ansan, Gyeonggi-do, 15588, Republic of Korea

† Electronic supplementary information (ESI) available. See DOI: https://doi.org/10.1039/d2bm00258b

‡ These authors contributed equally to this work.

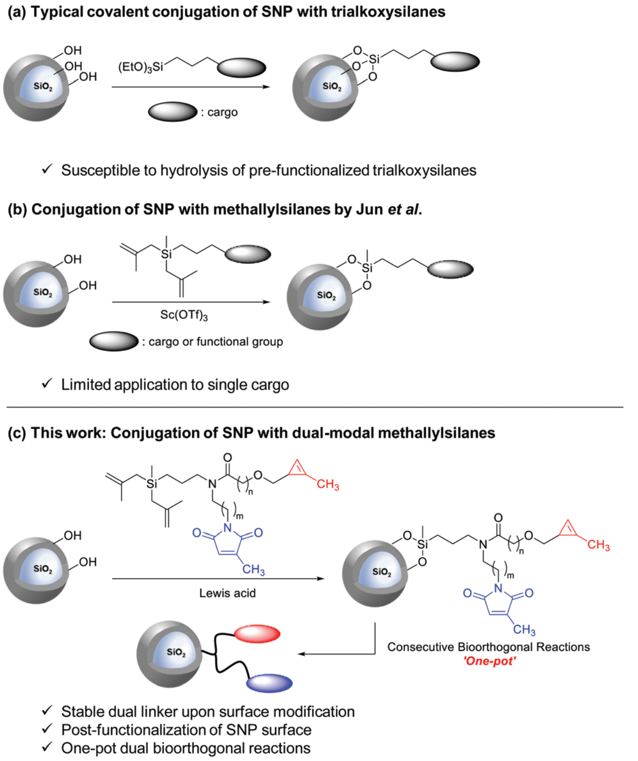

Fig. 1 A strategy for the construction of dual functional SNPs by covalent conjugation.

nides, and azides, which are preinstalled on allylsilanes, are grafted on the surface of silica and further applied to the incorporation of a desired biomolecule onto the silica by bioorthogonal reactions. For example, Jun *et al.*[8] demonstrated that methallylsilanes containing NHS-ester groups were integrated on silica surfaces in the presence of $Sc(OTf)_3$ to afford NHS-ester functionalized silica, which allowed the immobilization of glucose oxidase on silica *via* amide formation (Fig. 1b).

Owing to the high stability and versatility of allylsilanes, they are suitable substrates for preparing multifunctional SNPs *via* post-grafting. Accordingly, a novel methallylsilane conjugated with two bioorthogonal functional groups, methylcyclopropene and methylmaleimide, was designed (Fig. 1c). Methylcyclopropene, an electron-rich and strained alkene, can react with tetrazines *via* the inverse-electron demand Diels–Alder reaction (IEDDA),[9,10] whereas methylmaleimide acts as an effective Michael acceptor to undergo conjugate addition with reactive nucleophiles such as thiols and amines.[11] Accordingly, it is challenging to synthesize a reactive allylsilane with both bioorthogonal alkenes within one molecule and prove its effectiveness in SNP post-surface modification. Furthermore, if bioorthogonal reactions on the SNP surface occur independently without scrambling their functionality, this method will provide easy access to biomedical applications such as multimodal imaging or theranostics through covalent conjugation.[12]

In this study, we report the synthesis of bifunctional SNPs using methallylsilanes with a novel bioorthogonal dual linker as a post-grafting precursor and its application to multimodal *in vivo* imaging.

Results and discussion

The current study began with the synthesis of maleimide-conjugated methallylsilane **6** and cyclopropene **11**, as shown in Scheme 1. According to a previously reported procedure,[7f] we prepared chloroalkyl bismethallylsilane **2**, which was converted to tertiary amide **6** by alkylation with azido amine **3**, followed by an amide coupling reaction of the corresponding amine **4** with maleimide-conjugated acid **5**. The use of methyl-substituted maleimide is crucial for preventing undesirable cycloaddition between azide and maleimide during amide coupling.[13] Next, cyclopropenation of TMS-propyne with diazoacetate in the presence of $Rh(OAc)_4$ and subsequent DIBAL reduction yielded methylcyclopropenyl methyl alcohol **8**, which was treated with carbonyl diimidazole (CDI) and aminoalkyl ester to yield methylcyclopropenyl ester **9**. Finally, hydrolysis of **9** under basic conditions and concomitant removal of the trimethylsilyl group produced acid **11** in high yield.

To conjugate the azide moiety of **6** with acid **11** using amide coupling reagents, the reduction of azide to primary amine was required. However, we suspected that the direct formation of the corresponding amine would cause an intra- or intermolecular conjugate addition of the resulting amine to

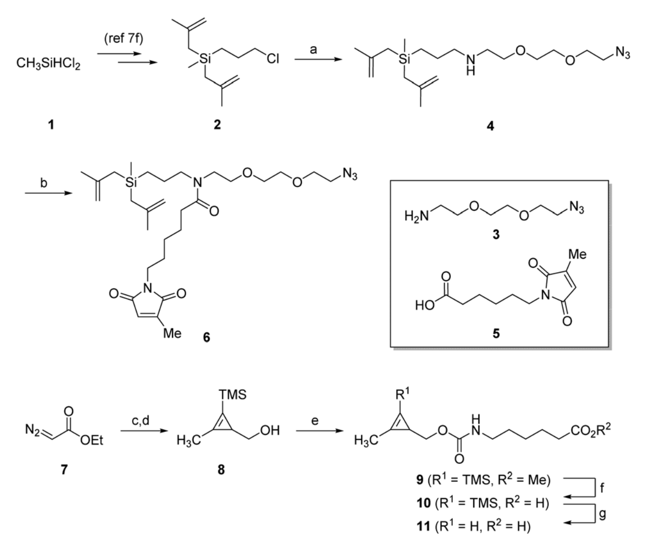

Scheme 1 Synthesis of maleimide conjugated allylsilane **6** and cyclopropene conjugated acid **11**. Reagents and conditions: (a) amine **3**, K_2CO_3 (2.0 equiv.), 80 °C, 58%; (b) acid **5**, EDCI (1.2 equiv.), DMAP (1.0 equiv.), CH_2Cl, rt, 78%; (c) Me–C≡C-TMS, $Rh_2(OAc)_4$ (0.01 equiv.), CH_2Cl_2, rt, 44%; (d) DIBAL (2.0 equiv.), Et_2O, 0 °C, 85%; (e) (i) CDI (1.1 equiv.), THF, rt; (ii) $MeO_2C(CH_2)_5NH_3Cl$, Et_3N (2.0 equiv.), DMF, 50 °C, 51%; (f) KOH (3.0 equiv.), $MeOH/H_2O$ (4 : 1), 0 °C; (g) TBAF (3.0 equiv.), THF, rt, 95% (2 steps).

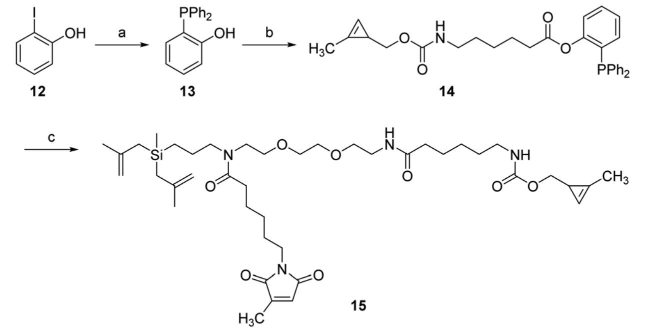

Scheme 2 Synthesis of allylsilane **15** with dual bioorthogonal linkers *via* traceless Staudinger ligation. Reagents and conditions: (a) Ph_2PH (1.0 equiv.), $Pd(OAc)_2$ (0.03 equiv.), NaOAc (1.0 equiv.), DMAc, 110 °C, 71%; (b) **11**, EDCI (1.4 equiv.), DMAP (1.0 equiv.), DMAc, 110 °C, 58%; (c) **6**, H_2O (3.0 equiv.), THF, 40 °C, 54%.

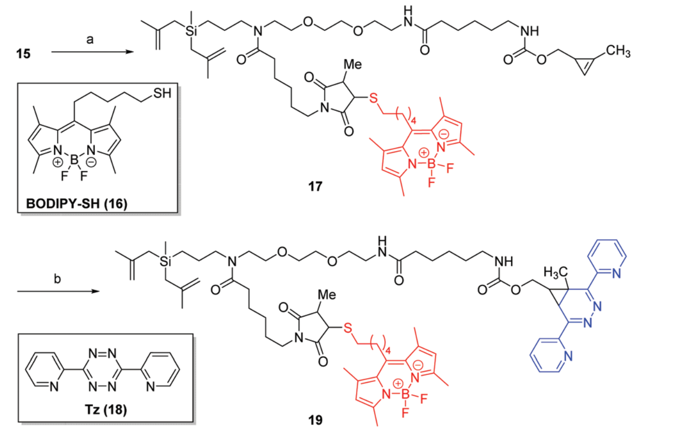

Scheme 3 Sequential bioorthogonal reactions of linker **15** with **16** and **18**. Reagents and conditions: (a) **16** (1.0 equiv.), Et_3N (0.03 equiv.), CH_2Cl_2, rt, 80%; (b) **18** (1.0 equiv.), CH_3CN, 87%.

the terminal maleimide group. Alternatively, inspired by 'traceless' Staudinger ligation developed by Bertozzi group,[14] we attempted direct conjugation of azide **6** with acid derivative **14**, which was prepared from esterification of **11** with 2-(diphenylphosphino)phenol **13** (Scheme 2). Although this ligation method has been used in several peptide syntheses, optimizing the reaction conditions is difficult due to aerobic oxidation of the phosphine precursor and undesirable hydrolysis of the iminophosphorane intermediate.[15] The reaction failed to produce the desired product **15** when water was initially added to a mixture of **6** and **14** in THF. Instead, amide **15** was observed when the mixture of **6** and **14** in THF was stirred at 40 °C for 12 h and then treated with a small amount of water. This result indicates that a certain time interval is required for forming imimophosphorane before hydrolysis. After investigating the optimal reaction conditions (see Table S1 in the ESI†), the reaction was found to proceed smoothly in the presence of water (3.0 equiv.) at 40 °C for 24 h to yield the desired silane **15** possessing two bioorthogonal functional groups in 54% yield.

Having synthesized dual linker conjugated silane **15**, verifying the reactivity and tolerance of both terminal alkenes of silane **15** to each bioorthogonal reaction before the surface modification of SNPs with **15** was necessary. Accordingly, the sequential bioorthogonal reactions of **15** with BODIPY dye **16**[16] and bipyridyl tetrazine **18**,[9b] as shown in Scheme 3 were examined. Conjugate addition of **16** to **15** at room temperature efficiently produced compound **17**, which was subjected to cycloaddition with **18** to produce cycloadduct **19** in high yield. Products **17** and **19** were sufficiently stable for isolation by flash column chromatography, and their structures were characterized by ^{1}H NMR, ^{13}C NMR, and LC/MS analyses. Additionally, the optical properties of **19** were determined and the reaction kinetics of tetrazine cycloaddition were estimated by measuring the UV absorbance of tetrazine **18** (Fig. S1†). The results established the excitation and emission wavelengths of **19** as 494 and 503 nm, respectively. The reaction between BODIPY conjugated linker **17** and tetrazine **18** exhibited relatively fast kinetics with a rate constant of $k = 4.3 \times 10^{-2}$ M^{-1} s^{-1}, which is comparable to that of a similar reaction.[10a]

Next, the surface modification of silica with dual linker **15** was investigated, as shown in Fig. 2. Considering the biomedical application of silica nanoparticles to biodistribution (*vide infra*) SNPs with monodisperse particle sizes smaller than 50 nm were selected.[17] Silica nanoparticles of controlled size were first prepared using the modified Stöber method (see the ESI† for details). Conjugation of freshly prepared SNPs (size was analyzed by DLS) with dual linker **15** was attempted. Despite linker **15** bearing two additional reactive alkenes, siloxane formation in the presence of 3 mol% $Sc(OTf)_3$ smoothly occurred to yield the desired SNP **20**. Upon completion of the reaction, surface-modified SNP **20** was collected by centrifu-

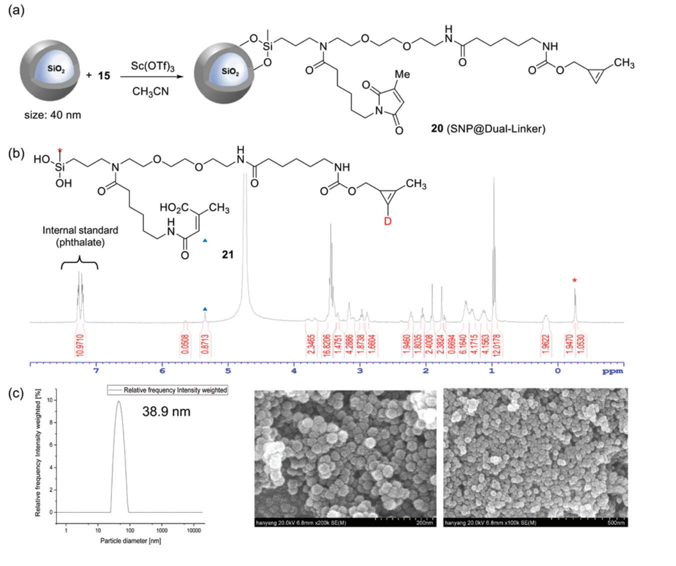

Fig. 2 Integration of methallylsilane **15** to SNPs. (a) Synthesis of linker-grafted SNP **20**; (b) Structure and ^{1}H NMR spectrum of compound **21**; (c) DLS graph of SNP **20** and SEM images before and after integration of linker **15** on the surface of SNPs.

gation, and the supernatant was removed. The isolated SNP **20** was washed with water and redispersed in acetonitrile three times, which produced a colloidal solution of **20** without aggregation. The size and shape of the surface-modified SNP **20** were characterized using DLS and SEM (Fig. 2). To further characterize the covalently bound linker on SNP **20**, NMR experiments[18] were performed, as shown in Fig. 2. The dried SNP **20** was dispersed in D_2O and treated with NaOD to disrupt silica nanoparticles to release silanol **22** in solution. No observation of particles in the DLS experiment indicated that silica nanoparticle **20** fully decomposed. The structure of compound **21** was determined by ^{1}H NMR and MS analyses. Interestingly, the ^{1}H NMR spectrum showed that the maleimide group was transformed to enoic acid under basic hydrolysis, and the proton on the cyclopropane ring was replaced by deuterium.[19] The proton signal at the silicon atom α-position was used to estimate the loading efficacy of the linker on the silica surface. The integrated intensity of the methyl protons attached to silicon was compared with that of the protons derived from potassium phthalate, an internal standard. The result indicated that the surface coverage of **20** by organic linker is 0.75 molecules per nm^2 (see the ESI† for calculation).

Since the installation of linker **15** on the SNP surface was confirmed, the bioorthogonal reactions used in Scheme 3 were applied to the linker-conjugated SNPs, as shown in Fig. 3. The dispersion of the dual linker-doped silica **20** in CH_3CN was treated with BODIPY dye **16** in the presence of triethylamine, followed by the consecutive addition of tetrazine **18** in *one pot* to yield dual functional SNP **22**. After the solvent was exchanged with water and acetonitrile three times, the purified SNP dispersion **22** was characterized by DLS, SEM, and fluorescence spectroscopy. The DLS and SEM results showed that the size of the functionalized SNP **22** was consistently maintained (40 nm) without particle aggregation. The optical property data of **22** in CH_3CN exhibited only a small red-shift compared with free silane **19**.[20] Furthermore, a kinetic study revealed that the rate of tetrazine cycloaddition on the SNP surface is slower than that of the reaction with the free linker **17** because of steric interference of the silica surface with the bioorthogonal reactions.

To investigate the biological application of dual linker-conjugated SNPs in an *in vivo* system, a biodistribution study using dual-imaging probes conjugated with a fluorophore and a radioactive isotope was performed (Scheme 4 and Fig. 4). Accordingly, a cyanine dye (Cy5.5) was applied to facilitate optical bioimaging since near-infrared (NIR) fluorescence shows relatively good tissue penetration and low background signal.[21] We also used iodine-125 as a source of the positron emission tomographic (PET) bioimaging probe, which could accurately visualize the biodistribution of SNPs in various tissues or organs *in vivo* regardless of tissue penetration depth. For the synthesis of radioactive tetrazine, we used an oxidative halo destannylation, recently developed by Valliant *et al.*,[22] to introduce ^{125}I into the pyridine moiety. Starting from 2-cyano-4-iodopyrdine **23**, iodopyrdinyl dihydrotetrazine **24** was prepared using an excess amount of hydrazine and sulfur, which was transformed to trimethylstannyl-substituted dihydrotetrazine **25** in high yield by a palladium-catalyzed coupling reaction. After we explored the reaction conditions for iodination using cold sodium iodide, radiolabeling was achieved by adding Na^{125}I to a mixture of stannane **25** and iodogen under acidic conditions. This reaction was completed within 5 min at room temperature, and the corresponding [^{125}I]-iodinated tetrazine **26** was used in the next step without purification. Following the same one-pot procedure used for the synthesis of SNP **22** (Fig. 3a), the dual linker conjugated SNP **20** was first

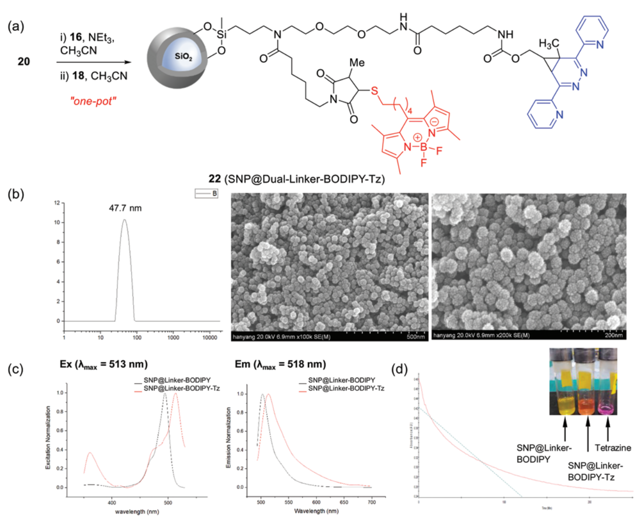

Fig. 3 Synthesis and characterization of dual functional SNP **22**. (a) One-pot sequential bioorthogonal reactions on the SNP surface; (b) DLS and SEM images; (c) excitation and emission spectra of **22**; (d) UV absorbance intensity at 535 nm in cycloaddition of tetrazine **18** to SNP in CH_3CN.

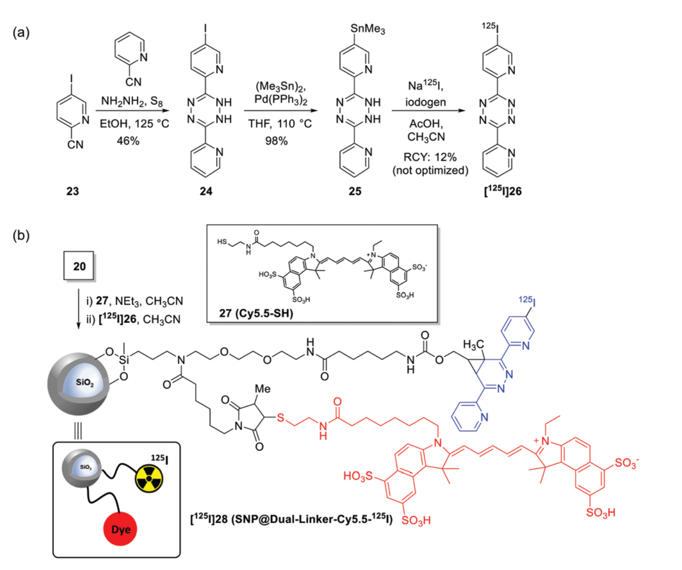

Scheme 4 Synthesis of dual-imaging silica nanoparticle **[^{125}I]28**. (a) Synthesis of ^{125}I-labeled tetrazine **26**; (b) one-pot synthesis of SNP conjugated with Cy 5.5 dye **27** and ^{125}I-tetrazine **26**.

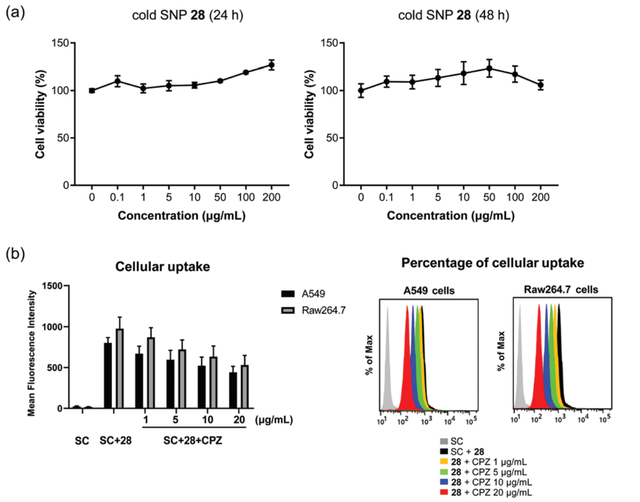

Fig. 4 Cell viability and cellular uptake of SNP **28**. (a) HEK293 T cells were incubated with SNP **28** for 24 h and 48 h respectively at the indicated concentrations; (b) SNP **28** (100 μg mL^{-1}) was incubated in A549 and Raw264.7 cells in the presence of the indicated CPZ concentrations (SC: solvent control, 0.1% DMSO).

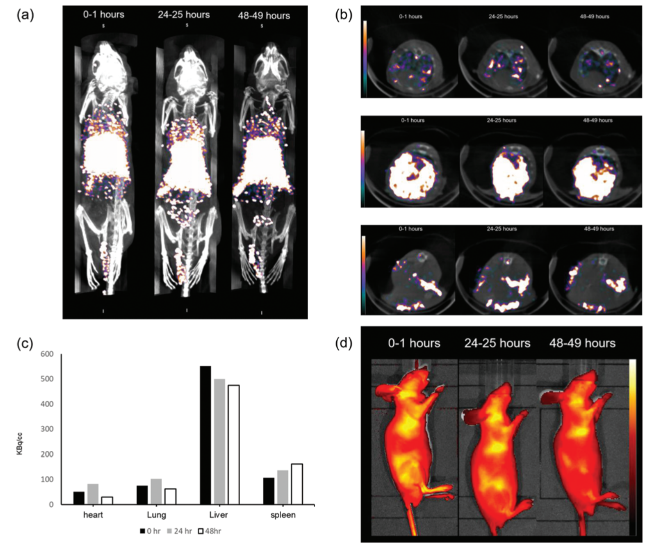

Fig. 5 Sequential *in vivo* biodistribution imaging data after intravenously administration of the Cy5.5 and ^{125}I covalently-labeled SNP **[^{125}I]28** to C57BL/6 mice. (a) Three-dimensional PET/CT images of whole body; (b) PET/CT images of transverse sections: lung (upper), liver (middle), and spleen (lower); (c) quantitative analysis of radioactivity in each organ of interest; (d) fluorescence images.

treated with thioalkyl cyanine dye **27**, followed by cycloaddition of [^{125}I]-tetrazine **26** to yield the desired SNP **[^{125}I]28**, in which both imaging probes were covalently conjugated. On the other hand, the same one-pot procedure was applied to the synthesis of cold SNP **28**, which was characterized by fluorescence, DLS and SEM (Fig. S2†).

Before the synthesized SNP **[^{125}I]28** was used in the *in vivo* experiment, the intrinsic cytotoxicity of cold SNP **28** was measured by the MTT assay,[23] which revealed that dual-modal SNP **28** induced no significant toxicity to HEK293 T cells, even at high concentrations (up to 200 μg mL^{-1}) for 48 h (Fig. 4a). The stability of cold SNP **28** was also tested in DI water, 1× PBS buffer and 10% FBS solution. The particle size and optical property of SNP **28** were not changed in the presence of the tested solutions, which indicated that SNP **28** is stable under physiological conditions (Fig. S3†). Additionally, the internalization of SNP **28** was investigated using chlorpromazine (CPZ) as an inhibitor of clathrin-mediated endocytosis. We observed that the SNP uptake by A549 and Raw264.7 decreased in dose-dependent manner by the clathrin inhibition (Fig. 4b). The result showed that clathrin-dependent endocytosis is the major mechanism of SNP **28** in cells.

Finally, a dispersed solution of Cy5.5 dye and ^{125}I-labeled silica nanoparticle **[^{125}I]28** in water was tested for systemic circulation *in vivo* (Fig. 5). All protocols were approved by the Institutional Animal Care and Use Committee of the Seoul National University Bundang Hospital (IACUC number BA-2009-304-085-04). The Ji Seok Young Research Center is fully accredited by the AAALAC. All animals were cared for in accordance with the ILAR Guide for the Care and Use of Laboratory Animals 8th Edition. The biodistribution of this SNP was determined at 24 and 48 h post-injection in C57Bl/6 mice. Immediately after the intravenous injection of SNP **[^{125}I]28**, most SNPs accumulated in the liver, but gradually cleared at 24 and 48 h. The SNPs in the lung and heart increased for 24 h and then decreased at 48 h, whereas the PET/CT signals in the spleen increased up to 48 h. With regard to the safety of SNP **[^{125}I]28**, the total activity that was detected in the PET/CT images showed no significant change for 48 h. In addition, no uptake of I-125 in the thyroid was observed, which indicated that there was no significant degradation of our dual-imaging SNPs up to 48 h. In the fluorescence experiment, most of the SNPs were detected in the liver. The biodistribution based on the fluorescence images was comparable to that found in the SPECT/CT images. The results established that our dual-modal imaging SNPs were tolerated under *in vivo* conditions for a long period of time.

Conclusions

We successfully developed new bifunctional silica nanoparticles, which can be covalently conjugated with heteroatom nucleophiles and tetrazines *via* one-pot consecutive bioorthogonal reactions. The synthesis of key methallylsilane **15** with cyclopropenes and maleimide was achieved by traceless Staudiger ligation. Methallylsilane **15**, which has two reactive alkenes, was introduced onto SNP surfaces smaller than 50 nm *via* Sc(OTf)$_3$-catalyzed siloxane formation. The dual linker-grafted SNP **20** was sufficiently stable to enable both conjugate addition and cycloaddition reactions in *one pot*. In addition, we demonstrated that dual functional SNP **[^{125}I]28** labeled with NIR dye and ^{125}I is applicable to biodistribution studies. Thus, we believe that the current covalent conjugation method using bioorthogonal dual linkers offers great potential for the development of multifunctional silica nanoparticles for a wide variety of biomedical applications.

Author contributions

Jaewoon Lee, Jeunghwan Kim, Incheol Heo, Su Jin Kim and Sein Jang collected experimental data and analysed the data. Kwang-Suk Jang, Chul-Su Yang, Youngbok Lee, and Won Cheol Yoo supervised the investigation and co-wrote the manuscript. Sun-Joon Min conceptualized the project methodology, wrote the original draft and supervised the investigation.

Conflicts of interest

The authors declare no competing financial interest.

Acknowledgements

This work was supported by the NRF grant funded by the Korea government (MSIP) (2020R1A4A4079870, 2021R1A4A5032463 and 2022R1A2C1005110). We would like to thank all members of the Basic Research Laboratory for critical reading and discussion of the manuscript.

Notes and references

1 (*a*) F. Chen, G. Hableel, E. R. Zhao and J. V. Jokerst, *J. Colloid Interface Sci.*, 2018, **521**, 261–279; (*b*) J. Xie, S. Lee and X. Chen, *Adv. Drug Delivery Rev.*, 2010, **62**, 1064–1079.

2 (*a*) M. Ghezzi, S. Pescina, C. Padula, P. Santi, E. Del Favero, L. Cantù and S. Nicoli, *J. Controlled Release*, 2021, **332**, 312–336; (*b*) J. Yang and Y.-W. Yang, *Small*, 2020, **16**, 1906846; (*c*) N. Zhao, L. Yan, X. Zhao, X. Chen, A. Li, D. Zheng, X. Zhou, X. Dai and F.-J. Xu, *Chem. Rev.*, 2019, **119**, 1666–1762; (*d*) G. Chen, I. Roy, C. Yang and P. N. Prasad, *Chem. Rev.*, 2016, **116**, 2826–2885; (*e*) W. Q. Lim, S. Z. F. Phua, H. V. Xu, S. Sreejith and Y. Zhao, *Nanoscale*, 2016, **8**, 12510–12519; (*f*) D. Ling, N. Lee and T. Hyeon, *Acc. Chem. Res.*, 2015, **48**, 1276–1285; (*g*) J. Liu, W. Huang, Y. Pang and D. Yan, *Chem. Soc. Rev.*, 2015, **44**, 3942–3953; (*h*) T. Sun, Y. S. Zhang, B. Pang, D. C. Hyun, M. Yang and Y. Xia, *Angew. Chem., Int. Ed.*, 2014, **53**, 12320–12364; (*i*) C. Argyo, V. Weiss, C. Bräuchle and T. Bein, *Chem. Mater.*, 2013, **26**, 435–451; (*j*) S. Mura, J. Nicolas and P. Couvreur, *Nat. Mater.*, 2013, **12**, 991–1003.

3 (*a*) J. G. Croissant, K. S. Butler, J. I. Zink and C. J. Brinker, *Nat. Rev. Mater.*, 2020, **5**, 886–909; (*b*) M. M. Abeer, P. Rewatkar, Z. Qu, M. Talekar, F. Kleitz, R. Schmid, M. Lindén, T. Kumeria and A. Popat, *J. Controlled Release*, 2020, **326**, 544–555; (*c*) P. Gh Jeelani, P. Mulay, R. Venkat and C. Ramalingam, *Silicon*, 2020, **12**, 1337–1354; (*d*) J. G. Croissant, Y. Fatieiev and N. M. Khashab, *Adv. Mater.*, 2017, **29**, 1604634; (*e*) L. Tang and J. Cheng, *Nano Today*, 2013, **8**, 290–312; (*f*) M. S. Bradbury, E. Phillips, P. H. Montero, S. M. Cheal, H. Stambuk, J. C. Durack, C. T. Sofocleous, R. J. Meester, U. Wiesner and S. Patel, *Integr. Biol.*, 2013, **5**, 74–86; (*g*) Z. Xu, D. Wang, M. Guan, X. Liu, Y. Yang, D. Wei, C. Zhao and H. Zhang, *ACS Appl. Mater. Interfaces*, 2012, **4**, 3424–3431; (*h*) J.-H. Park, L. Gu, G. Von Maltzahn, E. Ruoslahti, S. N. Bhatia and M. J. Sailor, *Nat. Mater.*, 2009, **8**, 331–336.

4 (*a*) F. Chen, B. Madajewski, K. Ma, D. K. Zanoni, H. Stambuk, M. Z. Turker, S. Monette, L. Zhang, B. Yoo, P. Chen, R. J. C. Meester, S. de Jonge, P. Montero, E. Phillips, T. P. Quinn, M. Gönen, S. Sequeira, E. de Stanchina, P. Zanzonico, U. Wiesner, S. G. Patel and M. S. Bradbury, *Sci. Adv.*, 2019, **5**, eaax5208; (*b*) K. Ma, D. Zhang, Y. Cong and U. Wiesner, *Chem. Mater.*, 2016, **28**, 1537–1545; (*c*) D. Kudela, S. A. Smith, A. May-Masnou, G. B. Braun, A. Pallaoro, C. K. Nguyen, T. T. Chuong, S. Nownes, R. Allen and N. R. Parker, *Angew. Chem., Int. Ed.*, 2015, **54**, 4018–4022; (*d*) A. Bumb, S. K. Sarkar, N. Billington, M. W. Brechbiel and K. C. Neuman, *J. Am. Chem. Soc.*, 2013, **135**, 7815–7818; (*e*) T. Ribeiro, S. Raja, A. S. Rodrigues, F. Fernandes, J. P. S. Farinha and C. Baleizão, *RSC Adv.*, 2013, **3**, 9171–9174; (*f*) B. Chen, M. Zuberi, R. B. Borgens and Y. Cho, *J. Biol. Eng.*, 2012, **6**, 1–8; (*g*) G. Alberto, G. Caputo, G. Viscardi, S. Coluccia and G. Martra, *Chem. Mater.*, 2012, **24**, 2792–2801; (*h*) S.-W. Ha, C. E. Camalier, G. R. Beck Jr. and J.-K. Lee, *Chem. Commun.*, 2009, 2881–2883.

5 (*a*) Z. Xu, X. Ma, Y.-E. Gao, M. Hou, P. Xue, C. M. Li and Y. Kang, *Mater. Chem. Front.*, 2017, **1**, 1257–1272; (*b*) X. D. Wang, K. S. Rabe, I. Ahmed and C. M. Niemeyer, *Adv. Mater.*, 2015, **27**, 7945–7950; (*c*) S. Bonacchi, D. Genovese, R. Juris, M. Montalti, L. Prodi, E. Rampazzo and N. Zaccheroni, *Angew. Chem., Int. Ed.*, 2011, **50**, 4056–4066; (*d*) S. Legrand, A. Catheline, L. Kind, E. C. Constable, C. E. House-croft, L. Landmann, P. Banse, U. Pielesa and A. Wirth-Heller, *New J. Chem.*, 2008, **32**, 588–593; (*e*) R. P. Bagwe, L. R. Hilliard and W. Tan, *Langmuir*, 2006, **22**, 4357–4362.

6 (*a*) A. Y. Fadeev and T. J. McCarthy, *Langmuir*, 2000, **16**, 7268–7274; (*b*) T. Shimada, K. Aoki, Y. Shinoda, T. Nakamura, N. Tokunaga, S. Inagaki and T. Hayashi, *J. Am. Chem. Soc.*, 2003, **125**, 4688–4689; (*c*) K. Aoki, T. Shimada and T. Hayashi, *Tetrahedron: Asymmetry*, 2004, **15**, 1771–1777; (*d*) M. P. Kapoor, S. Inagaki, S. Ikeda, K. Kakiuchi, M. Suda and T. Shimada, *J. Am. Chem. Soc.*, 2005, **127**, 8174–8178; (*e*) Y. Wang, S. Hu and W. J. Brittain, *Macromolecules*, 2006, **39**, 5675–5678; (*f*) Y. Maegawa, T. Nagano, T. Yabuno, H. Nakagawa and T. Shimada, *Tetrahedron*, 2007, **63**, 11467–11474.

7 (*a*) T. Morita, Y. Okamoto and H. Sakurai, *Tetrahedron Lett.*, 1980, **21**, 835–838; (*b*) A. Hosomi and H. Sakurai, *Chem. Lett.*, 1981, 85–88; (*c*) G. A. Olah, A. Husain, B. G. B. Gupta, G. F. Salem and S. C. Narang, *J. Org. Chem.*, 1981, **46**, 5212–5214; (*d*) G. A. Olah, A. Husain and B. P. Singh, *Synthesis*,

1983, 892–895; (*e*) T. Suzuki, T. Watahiki and T. Oriyama, *Tetrahedron Lett.*, 2000, **41**, 8903–8906; (*f*) Y.-R. Yeon, Y. J. Park, J.-S. Lee, J.-W. Park, S.-G. Kang and C.-H. Jun, *Angew. Chem., Int. Ed.*, 2008, **47**, 109–112; (*g*) J.-W. Park, Y. J. Park and C.-H. Jun, *Chem. Commun.*, 2011, **47**, 4860–4871.

8 R.-Y. Choi, C.-H. Lee and C.-H. Jun, *Org. Lett.*, 2018, **20**, 2972–2975.

9 (*a*) N. K. Devaraj and R. Weissleder, *Acc. Chem. Res.*, 2011, **44**, 816–827; (*b*) M. L. Blackman, M. Royzen and J. M. Fox, *J. Am. Chem. Soc.*, 2008, **130**, 13518–13519.

10 (*a*) D. M. Patterson, L. A. Nazarova, B. Xie, D. N. Kamber and J. A. Prescher, *J. Am. Chem. Soc.*, 2012, **134**, 18638–18643; (*b*) D. N. Kamber, L. A. Nazarova, Y. Liang, S. A. Lopez, D. M. Patterson, H.-W. Shih, K. N. Houk and J. A. Prescher, *J. Am. Chem. Soc.*, 2013, **135**, 13680–13683; (*c*) J. Šečkutė, J. Yang and N. K. Devaraj, *Nucleic Acids Res.*, 2013, **41**, e148.

11 (*a*) J. M. J. M. Ravasco, H. Faustino, A. Trindade and P. M. P. Gois, *Chem. – Eur. J.*, 2019, **25**, 43–59; (*b*) K. Renault, J. W. Fredy, P. Y. Renard and C. Sabot, *Bioconjugate Chem.*, 2018, **29**, 2497–2513; (*c*) P. Adumeau, S. K. Sharma, C. Brent and B. M. Zeglis, *Mol. Imaging Biol.*, 2016, **18**, 1–17.

12 J. Gea, Q. Zhangb, J. Zenga, Z. Gub and M. Gao, *Biomaterials*, 2020, **228**, 119553.

13 H.-Z. Zhu, G. Wang, H.-L. Wei, H.-J. Chu and J. Zhu, *Macromol. Res.*, 2016, **24**, 793–799.

14 E. Saxon, J. I. Armstrong and C. R. Bertozzi, *Org. Lett.*, 2000, **2**, 2141–2143.

15 T. K. Heiss, R. S. Dorn and J. A. Prescher, *Chem. Rev.*, 2021, **121**, 6802–6849.

16 F. Heisig, S. Gollos, S. J. Freudenthal, A. El-Tayeb, J. Iqbal and C. E. Müller, *J. Fluoresc.*, 2014, **24**, 213–230.

17 P. Dogra, N. L. Adolphi, Z. Wang, Y. S. Lin, K. S. Butler, P. N. Durfee, J. G. Croissant, A. Noureddine, E. N. Coker, E. L. Bearer, V. Cristini and C. J. Brinker, *Nat. Commun.*, 2018, **9**, 4551.

18 (*a*) C. I. C. Crucho, C. Baleizão and J. P. S. Farinha, *Anal. Chem.*, 2017, **89**, 681–687; (*b*) D. R. Hristov, L. Rocks, P. M. Kelly, S. S. Thomas, A. S. Pitek, P. Verderio, E. Mahon and K. A. Dawson, *Sci. Rep.*, 2015, **5**, 17040.

19 A. Fattahi, R. E. McCarthy, M. R. Ahmad and S. R. Kass, *J. Am. Chem. Soc.*, 2003, **125**, 11746–11750.

20 D. Ma, A. J. Kell, S. Tan, Z. J. Jakubek and B. Simard, *J. Phys. Chem. C*, 2009, **113**, 15974–15981.

21 (*a*) G. Hong, A. L. Antaris and H. Dai, *Nat. Biomed. Eng.*, 2017, **1**, 0010; (*b*) S. Wang, W. X. Ren, J.-T. Hou, M. Won, J. An, X. Chen, J. Shu and J. S. Kim, *Chem. Soc. Rev.*, 2021, **50**, 8887–8902; (*c*) H. W. Lee, D. J. Lee and C. S. Lim, *Bull. Korean Chem. Soc.*, 2021, **42**, 1184–1190.

22 (*a*) S. A. Albu, S. A. Al-Karmi, A. Vito, J. P. K. Dzandzi, A. Zlitni, D. Beckford-Vera, M. Blacker, N. Janzen, R. M. Patel, A. Capretta and J. F. Valliant, *Bioconjugate Chem.*, 2016, **27**, 207–216; (*b*) For a recent review of radioiodination, see: E. Dubost, H. McErlain, V. Babin, A. Sutherland and T. Cailly, *J. Org. Chem.*, 2020, **85**, 8300–8310.

23 S. Y. Park, S. A. Yoon and M. H. Lee, *Bull. Korean Chem. Soc.*, 2021, **42**, 119–123.